

# NEW INSIGHTS INTO THE FISSION PROCESS BY THE STUDY OF RELATIVISTIC NUCLEAR COLLISIONS

ALEKSANDRA KELIĆ and KARL-HEINZ SCHMIDT  
*for CHARMS Collaboration\**

*GSI, Planckstr. 1, Darmstadt, D-64291, Germany*

An experimental and theoretical campaign dedicated to a better understanding of the fission process has been started at GSI several years ago. The waste amount of data measured at GSI gave new information on different aspects of the nuclear-fission process, such as nuclear viscosity at small deformation, transient effects, influence of shell effects on mass- and charge-division in fission, pairing correlations. All this lead to a development of a model, which proved successful in describing fragment formation in spallation and fragmentation reactions.

## 1. Introduction

Since some years, reactions at relativistic energies induced by light particles (spallation reactions) and heavy ions (fragmentation reactions) have gained a renewed interest for several reasons. For example, spallation reactions lead to the production of unstable nuclei and are actually exploited in ISOL-type radioactive-beam facilities [1,2]. They are also planned to be used in the so-called Accelerator Driven System [3,4] as an intense neutron source. Additionally, spallation reactions are of interest for astrophysics, e.g. nuclide production via interactions of cosmic rays with interstellar medium [5,6,7], space technologies [8,9], and biology and medicine [10,11]. Moreover, relativistic nuclear collisions proved to be an excellent tool for studying basic properties of nuclear matter, such as nuclear equation-of-state or thermal instabilities in heated nuclei [12]. Therefore, it is of prime interest to understand the different mechanisms leading to the production of final residues in relativistic nuclear collisions.

In case of heavy nuclei, two mechanisms compete during the deexcitation path of excited prefragments formed in primary interactions between target nuclei and incoming relativistic projectiles – evaporation and fission. While evaporation can rather well be described using different approaches, e.g. Weisskopf-Ewing or Hauser-Feschbach models, fission still remains a puzzle although nuclear fission is the most intensively studied nuclear reaction. One of

---

\* <http://www.gsi.de/charms/>

the reasons is that only few nuclei have been investigated up to very recently. Experiments were restricted to spontaneously fissioning isotopes and primordial or long-lived target nuclei. Except for measurements performed at Lohengrin [13], where both the mass and nuclear charge of the light fission group have been measured with high resolution, from most of experiments only information on mass distributions with low resolution is available. Additional problems arise from the theoretical point of view. The fission process corresponds to a large-scale collective motion, where static, e.g. nuclear potential at large deformations, as well as dynamical, e.g. nuclear viscosity, properties play an important role in the description of nuclear fission. Unfortunately, one still does not have a clear and unique understanding of these properties.

To this goal, an experimental and theoretical campaign has been started at GSI. Fission fragments formed in spallation and fragmentation of different nuclei, e.g.  $^{238}\text{U}$ ,  $^{208}\text{Pb}$ ,  $^{197}\text{Au}$ , were identified using the inverse-kinematics method in which both mass and nuclear charge and their velocities have been measured with high precision. Moreover, the fragments formed in fission after electromagnetic- and nuclear-excitation of secondary projectiles have also been measured. The waste amount of measured data gave new information on different aspects of the nuclear-fission process, such as nuclear viscosity at small deformation, transient effects, influence of shell effects on mass- and charge-division in fission, pairing correlations.

In this contribution, experimental details of two approaches developed at GSI will be given. Some aspects of the fission process will also be discussed. More details on the nuclear dissipation and transient effects will be given in the contribution of Christelle Schmitt to this proceedings.

## 2. Experiment

At GSI-Darmstadt, an innovative experimental approach based on the inverse-kinematics method has been developed. Experiments in inverse kinematics are performed at relativistic energy shooting a heavy-ion beam into a target. Under these experimental conditions, the produced fragment escapes the target strongly focused in forward direction and is detected in-flight prior to its  $\beta$ -decay.

Within this approach, two methods have been applied: (1) High-resolution experiments, where only one fission fragment is measured, but is fully identified in the mass and atomic number using the magnetic spectrometer FRS. At the same time, information on the reaction kinematics is available. (2) Full-acceptance experiments, where both fission fragments are detected, and identified in atomic number. Below, these two methods will be described in more details.

### 2.1. High-resolution experiments

The SIS18 heavy-ion accelerator of GSI is used to provide heavy-ion beams at energies up to 2 GeV per nucleon and with intensities up to  $10^{11}$  particles per spill. The primary-beam intensity is continuously monitored by a beam-intensity monitor based on secondary-electron emission [14,15]. The heavy-ion beam provided by the SIS18 impinges on a target, and residues produced in the target are identified using the Fragment Separator (FRS) [16] and the associated detector equipment, see Figure 1.

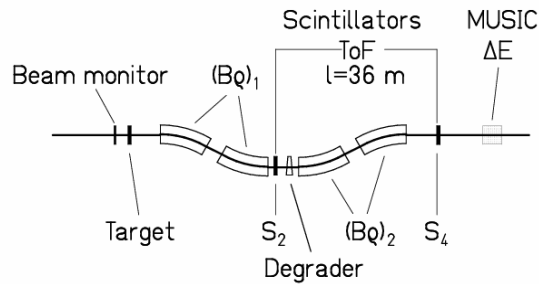


Figure 1 Schematic drawing of the fragment separator FRS with the detector equipment. For details see text.

The FRS is a two-stage magnetic spectrometer with a dispersive intermediate image plane (S<sub>2</sub>) and an achromatic final image plane (S<sub>4</sub>) with a momentum acceptance of 3% and an angular acceptance of about 15 mrad around the beam axis. Two position-sensitive plastic scintillators placed at S<sub>2</sub> and S<sub>4</sub>, respectively, provide the magnetic-rigidity ( $B\rho$ ) and the time-of-flight measurements, which allow determining the mass-over-charge ratio of the particles. The nuclear charges are deduced from the energy loss in an ionization chamber (MUSIC) with a resolution  $\Delta Z = 0.4$  (FWHM). Combining this information with the mass-over-charge ratio, a complete nuclide identification can be performed. The resulting mass resolving power is  $\Delta A/A \sim 2.5 \cdot 10^{-3}$ . One example of the excellent resolution in mass and nuclear charge is given in Figure 2. The momentum distribution of each residue is obtained from the measurement of the magnetic rigidity  $B\rho$  in the first half of the FRS. In this way, the resolution with which the momentum is obtained amounts to  $\sim 5 \cdot 10^{-4}$ , and is improved by about one order of magnitude as compared to the resolution obtained from the TOF measurement. In a given experiment, usually more than 100 different values of the magnetic fields are needed in order to cover all the produced residues and to construct the full momentum distribution of each residue for one projectile-target combination. The re-construction of the full momentum distribution allows for disentangling reaction products formed in

fragmentation and fission reactions due to their different kinematic properties [17,18].

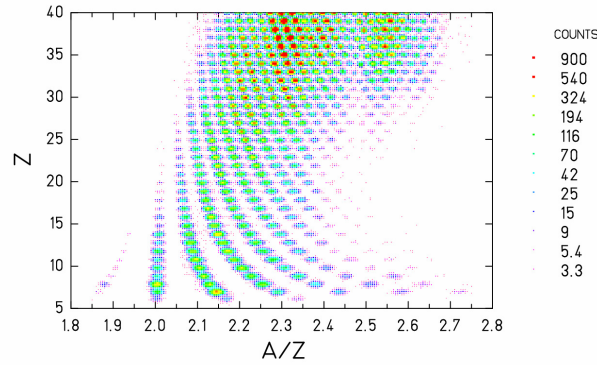


Figure 2 Identification pattern – nuclear charge versus mass-over-charge ratio – for the reaction  $^{238}\text{U}$  (1 A GeV) +  $^1\text{H}$ . Each spot represents one nuclide. The color code gives, on the logarithmic scale, the number of counts for each nuclide. Only a part ( $Z \leq 40$ ) of the produced nuclides is shown. Figure taken from ref. [17].

The production cross section of a specific nuclide is obtained from its production rate given by the surface below the peak in the corresponding momentum distribution corrected for the dead time of the data-acquisition system, for losses due to secondary reactions in different layers of matter in the beam line, for losses coming from the rejections of the incompletely stripped ions from the data analysis, and also normalizing to the number of counts in the beam-current monitor and to the number of target atoms per area. Details on these corrections are given in ref. [19]. Finally, one needs to correct the measured data for the limited angular acceptance of the FRS. This is done according to the procedure described in ref. [18]. As an example, in Fig. 3 production cross sections measured in the reaction  $^{238}\text{U}+^1\text{H}$  at 1 GeV per nucleon [17,20,21,22,23] are shown on the nuclide chart.

## 2.2. Full-acceptance experiments

In another type of experiments, the FRS is used to produce and guide the secondary beams to the dedicated experimental setup situated at the S4 area of the FRS. Secondary beams are produced in the interactions of a 1 A GeV  $^{238}\text{U}$  primary beam with a beryllium target. Some 70 secondary projectiles ranging from  $^{205}\text{At}$  to  $^{234}\text{U}$  were spatially separated and identified event-by-event using the FRS and the associated equipment (as described above). These nuclides were then sent to the secondary target situated at the exit of the FRS. Fission induced in nuclear and electromagnetic interactions of radioactive projectiles with the lead target was studied using the dedicated experimental set-up, see Figure 4. A double ionisation chamber allows for the detection of both fission fragments in

coincidence, and for the determination of their atomic numbers with a resolution of  $\Delta Z = 0.4$  (FWHM). A typical charge correlation spectrum is displayed in Figure 5. A detailed description of the experimental set-up can be found in ref. [24].

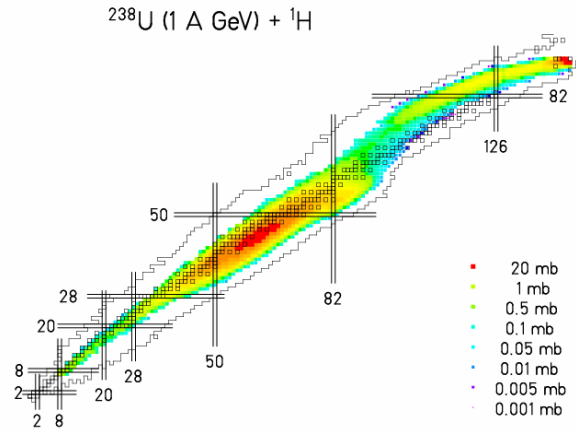


Figure 3 Residual nuclide cross sections for the reaction  $^{238}\text{U}+^1\text{H}$  at 1 GeV per nucleon [17,25,26,27,28] on a chart of the nuclides. Cross sections are given as a color code on the logarithmic scale. Primordial nuclei are marked by open squares, the outer line gives the range of known nuclides, and the shell closures are indicated by double lines.

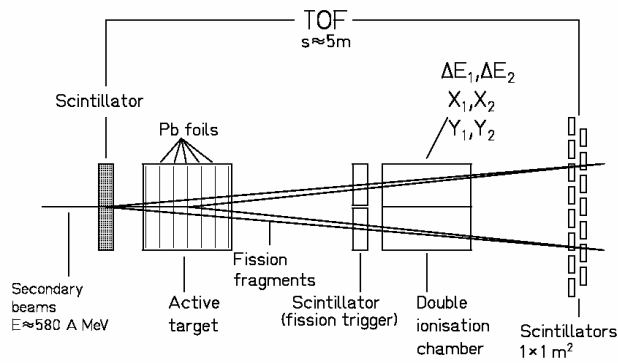


Figure 4 Experimental set-up for fission studies of secondary beams – the secondary beam separated and identified by the FRS (see Figure 1) enters the lead target. Fission fragments formed via nuclear and electromagnetic interactions are passing through a double ionization chamber, and are identified simultaneously in nuclear charge.

As an example, in Figure 6 are shown the charge distributions of fission fragments formed in electromagnetic-induced fission of several light actinides [24]. The transition from single-humped to double-humped charge distributions

when going from  $^{221}\text{Ac}$  to  $^{234}\text{U}$  is clearly visible. In the next session we will discuss these features in more details.

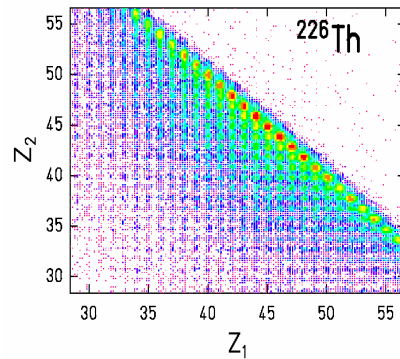


Figure 5 Correlation plot between nuclear charges of two fragments formed in fission of  $^{226}\text{Th}$ . Data taken from ref. [29].

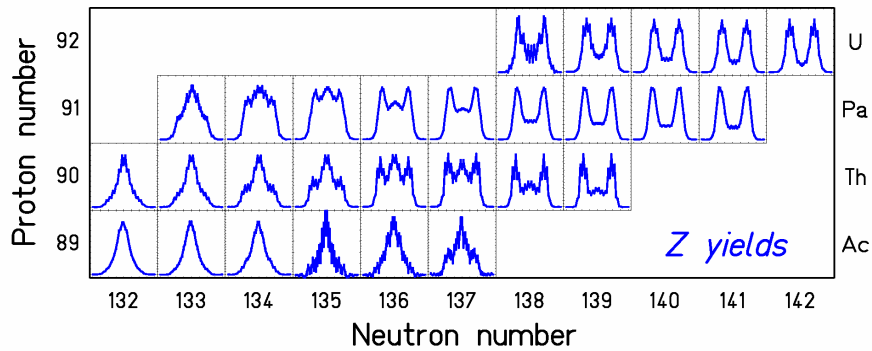


Figure 6 Nuclear-charge distributions of fragments formed in electromagnetic-induced fission of several secondary beams ranging from  $^{205}\text{At}$  and  $^{234}\text{U}$ . Data taken from ref. [24].

### 3. New information on the fission process

The large amount of experimental data obtained at GSI allows gaining new information on different fission-process properties, e.g. nuclear viscosity at small deformation [29,30,31,32,33,34], influence of shell effects on mass- and charge-division in fission [24,35,36,37], pairing correlations [38,39,40]. In the following, some of these properties will be discussed.

#### 3.1. Mass and charge division in fission

From the available experimental data on mass and/or charge splits in fission several observation can be made: while at high excitation energy the distributions of fission fragments are symmetric and very well described within

the liquid-drop model [41], at low excitation energy the influence of shell corrections and pairing correlations play an important role [24].

In the course of time, different approaches have been developed in order to reproduce and predict mass and charge splits in fission. One can divide them in two groups: Either the evolution of the fissioning system is described with a purely theoretical model or the measured observables are fitted by suitable functions with empirically determined parameters. The first approach is very challenging. These models are very important for improving our understanding of the fission process, but their ability for quantitative predictions seems to be still rather limited. In the second approach, mass and charge distributions are parameterized using more or less complicated mathematical formulas. This kind of approach is very adapted if one is interested in nuclei in regions where experimental data are available, but it is not reliable for extrapolations in unknown regions due to the lack of the essential physics.

In order to surmount these problems, we have chosen an intermediate approach, which is based on physical models but uses adjustments to experimental data. A preliminary version of the model was described in ref. [36]. In this semi-empirical approach, the transition from single-humped to double-humped fragment distributions is explained by macroscopic (defined by the fissioning nucleus) and microscopic (defined by the nascent fragments) properties of the potential-energy landscape near the outer saddle point. Macroscopic features of the potential-energy landscape are deduced from mass distributions at high excitation energy [41] and Langevin calculations [42], while microscopic features are based on shell-model calculations [43,44] and theoretical assumptions on washing out of shell effects [45]. The parameters describing the microscopic features in the potential are deduced from data on measured features of fission channels: nuclide yields, neutron yields,  $TKE$ . We use certain assumptions on the dynamics of fragment formation, i.e. that the mass division is already determined at the outer saddle point, while the  $N/Z$  degree of freedom is very fast compared to the motion from saddle-to-scission and is, therefore, determined at the scission point.

As an example for the application of this approach, we show in Figure 7 a comparison between experimental and model-calculated charge distributions of fragments formed in the electromagnetic-induced fission of several secondary beams ranging from  $^{220}\text{Ac}$  to  $^{234}\text{U}$  [24]. The transition from single- to triple- and then to double-humped fragment distributions is correctly described by the model. Please note that all calculations were performed with the same set of model parameters; no adjustment to individual systems has been done. This global aspect of the approach gives us confidence when extrapolating into regions where no experimental data are available, see e.g. [46,47].

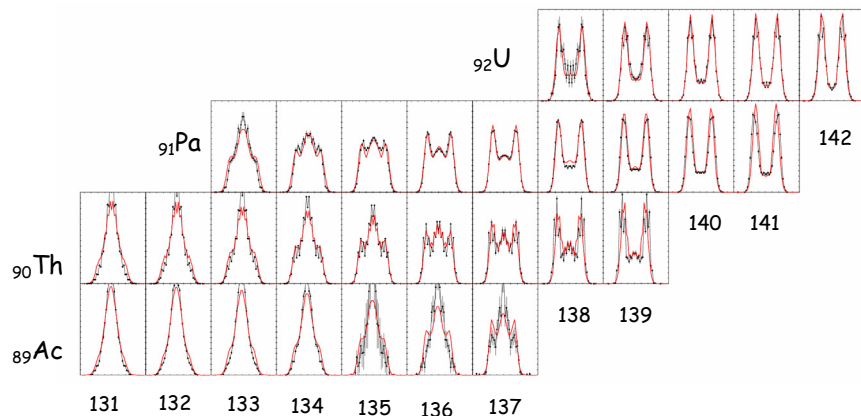


Figure 7 Comparison between measured (black dots) and calculated (red line) fission-fragment nuclear-charge distributions in the range  $Z = 24$  to  $Z = 65$  from  $^{220}\text{Ac}$  to  $^{234}\text{U}$  in electromagnetic-induced fission shown on a chart of the nuclides. Experimental data are taken from Ref. [24]. Calculations are performed with the GSI reaction model ABRABLA.

### 3.2. Nuclear viscosity

One of the basic properties of nuclear matter is the viscosity. It describes the coupling between intrinsic and collective degrees of freedom. Since fission corresponds to a typical large-scale motion process, it has been recognised as one of the most promising tools to investigate nuclear viscosity. To this goal, an experimental campaign has been started at GSI to investigate nuclear viscosity at small deformation based on measuring the nuclide distributions of fission products emerging from peripheral fragmentation reactions in inverse kinematics [29,48,49,50,51,52]. One of the common conclusions of these studies is that the motion up to the saddle point is over-damped. For the more detailed discussion on this topic see a contribution of Christelle Schmitt to this Conference.

### 3.3. Fission barriers

One of the most important ingredients for calculating fission probabilities is the height of the fission barrier. Unfortunately, experimental information on fission-barrier heights is only available for nuclei in a limited region of the nuclide chart. Therefore, for exotic heavy nuclei (e.g. in the super-heavy region or along the astrophysical r-process path) one has to rely on theoretically calculated barriers. In applications, mostly used models are of the macroscopic-

microscopic type, where the macroscopic contribution to the masses is based either on some liquid-drop, droplet or Thomas-Fermi model, while microscopic corrections are calculated separately, mostly using the Strutinsky method [53]. Due to the limited number of available experimental barriers, in any theoretical model, constraints on the parameters defining the dependence of the fission barrier on neutron excess are rather weak. This leads to large uncertainties in estimating the heights of the fission barriers of exotic nuclei.

Recently, we have performed a study on the behaviour of the macroscopic contribution to the fission barriers when extrapolating to very neutron-rich nuclei [54]. This study was based on the approach of Dahlinger *et al.* [55], where the predictions of the theoretical models were examined by means of a detailed analysis of the isotopic trends of ground-state and saddle-point masses. In order to test the consistency of these models, we study the difference between the experimental saddle-point mass and the macroscopic part of the saddle-point mass as predicted by the theoretical models. The difference between experimental and macroscopic mass,  $\delta U_{sadd}$  should correspond to the empirical shell-correction energy. It is well known that the shell-correction energy oscillates with deformation and neutron or proton number. If we consider deformations corresponding to the saddle-point configuration, then the oscillations in the microscopic corrections for heavy-nuclei region we are interested in are expected to have a period between about 10 ~ 30 neutrons depending on the single-particle potential used, see e.g. [56,57,58,59]. This means that, if we follow the isotopic trend of the shell-correction energy at the saddle point over a large enough region of neutron numbers, this quantity should show only local variations with the above given periodicity. Moreover, as the shell-correction energy at the saddle point is very small – below 1 – 2 MeV [60,61], these local variations should also be very small. In other words, the saddle-point shell-correction energy as a function of neutron number should show only local, periodical, variations with small amplitude; there should be no global tendencies, e.g. constant increase or decrease with neutron number.

We have used this criterion in Ref. [54] to test the macroscopic part of the different macroscopic-microscopic models. Using experimental ground-state masses [62] in combination with experimental fission barriers and different macroscopic models, we have calculated the quantity  $\delta U_{sadd}$  for a wide range of neutron numbers. If a model describes realistically the isotopic trend, the quantity  $\delta U_{sadd}$  will correspond to the shell-correction energy at the saddle point and will fulfil the above-mentioned condition, i.e. the slope of  $\delta U_{sadd}$  as a function of neutron number will be close to zero. On the contrary, if a model does not describe realistically the isotopic trend, then the quantity  $\delta U_{sadd}$  as a

function of neutron number will show global tendencies, like e.g. increase or decrease over a large range of neutron numbers.

For four studied models: the Droplet model [63], the Finite-range liquid drop model [64], the Thomas-Fermi model [60] and the Extended Thomas-Fermi model [65], the slopes of  $\delta U_{sadd}$  as a function of neutron number are shown in Figure 8 versus atomic number. For more details, see [54].

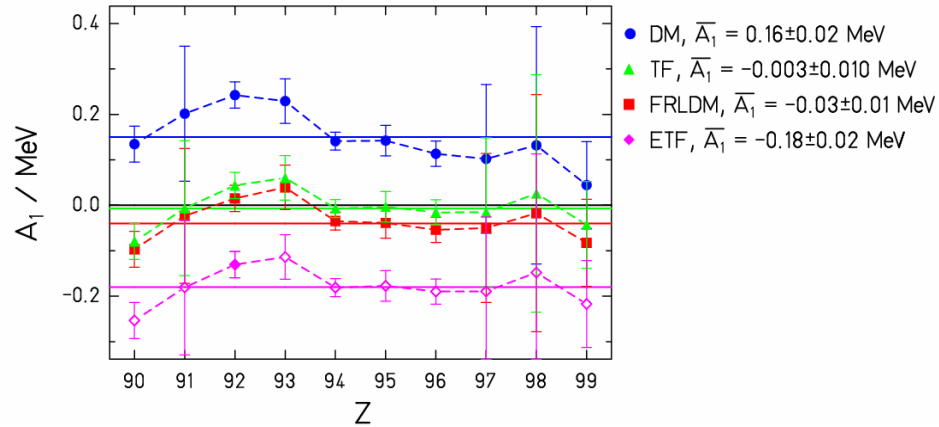


Figure 8 Slopes of  $\delta U_{sadd}$  as a function of the neutron excess are shown as a function of the nuclear charge number  $Z$  obtained for the droplet model (points), the Thomas-Fermi model (triangles), FRLDM (squares) and the extended Thomas-Fermi model (rhomboids); The full lines indicate the average values of the slopes. The average values are also given in the figure. Error bars originate from the experimental uncertainties in the fission-barrier heights. Dashed lines are drawn to guide the eye. For more details, see [54].

We can see from Figure 8 that the Thomas-Fermi and the Finite-range liquid drop model predict slopes which are very close to zero, while the Droplet and the Extended Thomas-Fermi model result in the slope values which are not consistent with zero.

The results of this study (see also [54]) show that the most realistic predictions are expected from the Thomas-Fermi model [60]. A similar conclusion can be made for the Finite-range liquid-drop model [64] while further improvements in the saddle-point mass predictions of the Droplet model [63] and the Extended Thomas-Fermi model [65] seem to be needed.

#### 4. Conclusions

Using an innovative experimental method developed at GSI a large amount of high-quality fission data has been accumulated. Measured production cross sections, mass and/or nuclear-charge distributions, and kinematical properties represent an excellent basis for a better understanding of different properties of

the fission process. Thanks to these data, new information on the nuclear viscosity, transient effects, shell effects and pairing correlations has been obtained, and the reaction model ABRABLA with high predictive power has been developed.

## References

---

1. <http://www94.web.cern.ch/ISOLDE>
2. <http://www.triumf.ca/welcome/>
3. C. Rubbia et al, Report CERN/AT/95-44/(ET) (1995).
4. C.D. Bowmann et al, Nucl. Instr. Meth. A320, 336 (1992).
5. R.C. Reedy et al, J. Geophys. Res 77, 537 (1972).
6. Th. Schiekkel et al, Nucl. Instr. Meth. B114, 91 (1996).
7. R. Michel and S. Neumann, Proceed. Intern. Conf. On Isotopes in the Solar System, Indian Academy of Science (Earth and Planetary Science) 107, 441 (1998).
8. S. Buchner et al, IEEE Trans. Nucl. Sci. 47, 705 (2000).
9. H.H.K. Tang and N. Olsson, Mat. Res. Soc. Bull. 28 (2003).
10. A. Wambersie et al, Radiat. Prot. Dosim. 31, 421 (1990).
11. D.T. Bartlett et al, Radiat. Res. Cong. Proc. 2, 719 (2000).
12. V.A. Karnaukov, Phys. Part. Nuclei 37, 165 (2006).
13. U. Quade et al, Nucl. Phys. A487, 1 (1988)
14. A.R. Jungahns et al, Nucl. Instr. Meth. A 370, 312 (1996).
15. B. Jurado et al, Nucl. Instr. Meth. A 483, 603 (2002).
16. H. Geissel et al, Nucl. Instr. Meth. B 70, 150 (1992).
17. M.V. Ricciardi et al, Phys. Rev. C 73, 014607 (2006).
18. J. Benlliure et al, Nucl. Instr. Meth. A 478, 493 (2002).
19. T. Enqvist et al, Nucl. Phys. A 686, 481 (2001).
20. M. Bernas et al, Nucl. Phys. A 765, 197 (2006).
21. M. Bernas et al, Nucl. Phys. A 725 213 (2003).
22. J. Taieb et al, Nucl. Phys. A 724, 413 (2003).
23. P. Armbruster et al, Phys. Rev. Lett. 93 212701 (2004).
24. K.-H. Schmidt et al, Nucl. Phys. A 665, 221 (2000).
25. M. Bernas et al, Nucl. Phys. A 765, 197 (2004).
26. M. Bernas et al, Nucl. Phys. A 725, 213 (2003).
27. J. Taieb et al, Nucl. Phys. A 724, 413 (2003).
28. P. Armbruster et al, Phys. Rev. Lett. 93, 212701 (2004).
29. Ch. Schmitt et al, in preparation; see also contribution of Ch. Schmitt to this Proceedings
30. B. Jurado et al, Phys. Lett. B533, 186 (2003).
31. B. Jurado et al, Phys. Rev. Lett. 93, 072501 (2004).
32. B. Jurado et al, Nucl. Phys. A757, 329 (2005).
33. B. Jurado et al, Nucl. Phys. A747,14 (2005).
34. J. Benlliure et al, Phys. Rev. C74, 014609 (2006).
35. S.I. Mulgin et al, Nucl. Phys. A640, 375 (1998).

- 
36. J. Benlliure, A. Grewe, M. de Jong, K.-H. Schmidt and S. Zhdanov, Nucl. Phys. A 628, 458 (1998).
  37. A.R. Junghans et al, Nucl. Phys. A629, 635 (1998).
  38. S. Steinhäuser et al, Nucl. Phys. A634, 89 (1998).
  39. F. Rejmund et al, Nucl. Phys. A678, 215 (2000).
  40. K.-H. Schmidt et al, in Proceedings of Third International Workshop on Nuclear Fission and Fission-Product Spectroscopy, Cadarache, France, May 11-14, 2005 (AIP Conference Proceedings, Vol. 798, New York, 2005, Editors: H. Goutte, H. Faust, G. Fioni, D. Goutte, ISBN 0-7354-0288-4)
  41. Ya. Rusanov et al., Phys. At. Nucl. 60, 683 (1997).
  42. P. N. Nadtochy, G. D. Adeev and A. V. Karpov, Phys. Rev. C 65, 064615 (2002).
  43. J. Maruhn and W. Greiner, Z. Phys. 251, 431 (1972).
  44. V. V. Pashkevich, Nucl. Phys. A 477, 1 (1988).
  45. A. V. Ignatyuk, G. N. Smirenkin and A. S. Tiskin, Yad. Fiz. 21, 485 (1975) (Sov. J. Nucl. Phys. 21, 255 (1975))
  46. A. Kelić, N. Zinner, E. Kolbe, K. Langanke and K.-H. Schmidt, Phys. Lett. B 616, 48 (2005).
  47. G. Martinez-Pinedo et al, in Proceedings of the International Symposium on Nuclear Astrophysics "Nuclei in the Cosmos - IX", CERN, Geneva, June 25-30, 2006, Proceedings of Science (<http://pos.sissa.it/>).
  48. B. Jurado et al, Phys. Lett. B533, 186 (2003).
  49. B. Jurado et al, Phys. Rev. Lett. 93, 072501 (2004).
  50. B. Jurado et al, Nucl. Phys. A757, 329 (2005).
  51. B. Jurado et al, Nucl. Phys. A747,14 (2005).
  52. J. Benlliure et al, Phys. Rev. C74, 014609 (2006).
  53. V.M. Strutinsky, Nucl. Phys. A 95, 420 (1967).
  54. A. Kelić and K.-H. Schmidt, Phys. Lett. B 642, 362 (2006).
  55. M. Dahlinger, D. Vermeulen and K.-H. Schmidt, Nucl. Phys. A 376, 94 (1982).
  56. D. Scharnweber, U. Mosel and W. Greiner, Phys. Rev. Lett. 24, 601 (1970).
  57. M. Bolsterli, E.O. Fiset, J.R. Nix and J.L. Norton, Phys. Rev. C 5, 1050 (1972).
  58. P. Möller and J.R. Nix, „Physics and Chemistry of Fission“, Proceedings of a conference at Rochester (IAEA, Vienna 1974), Volume 1, page103.
  59. J. Randrup, S.E. Larson, P. Möller, S.G Nilsson, K. Pomorski, A. Sobiczewski, Phys. Rev. C 13, 229 (1976).
  60. W.D. Myers and W.J. Swiatecki, Phys. Rev. C 60, 014606-1 (1999).
  61. K. Siwek-Wilczyńska, I. Skwira, and J. Wilczyński, Phys. Rev. C 72, 034605 (2005).
  62. G. Audi, A. H. Wapstra and C. Thibault, Nucl. Phys. A 729, 337 (2003).
  63. W.M. Howard and P. Möller, At. Data Nucl. Data Tables 25, 219 (1980).
  64. A.J. Sierk, Phys. Rev. C 33, 2039 (1986).
  65. A. Mamdouh, J.M. Pearson, M. Rayet and F. Tondeur, Nucl. Phys. A 679, 337 (2001).